

1   Supplementary Information for: Mafic Archean continental crust  
2   prohibited exhumation of orogenic UHP eclogite

3

4   **Richard M. Palin<sup>1</sup>\*, James D. P. Moore<sup>2,3</sup>, Zeming Zhang<sup>4</sup> and Guangyu Huang<sup>5</sup>**

5   <sup>1</sup>*Department of Earth Sciences, University of Oxford, Oxford, OX1 3AN, United Kingdom*

6   <sup>2</sup>*Earth Observatory of Singapore, Nanyang Technological University, Singapore*

7   <sup>3</sup>*Institute of Geophysics, SGEES, Victoria University of Wellington, Wellington, New Zealand*

8   <sup>4</sup>*Institute of Geology, Chinese Academy of Geological Sciences, Beijing 100037, China*

9   <sup>5</sup>*State Key Laboratory of Lithospheric Evolution, Institute of Geology and Geophysics, Chinese  
10   Academy of Sciences, Beijing 100029, China*

11

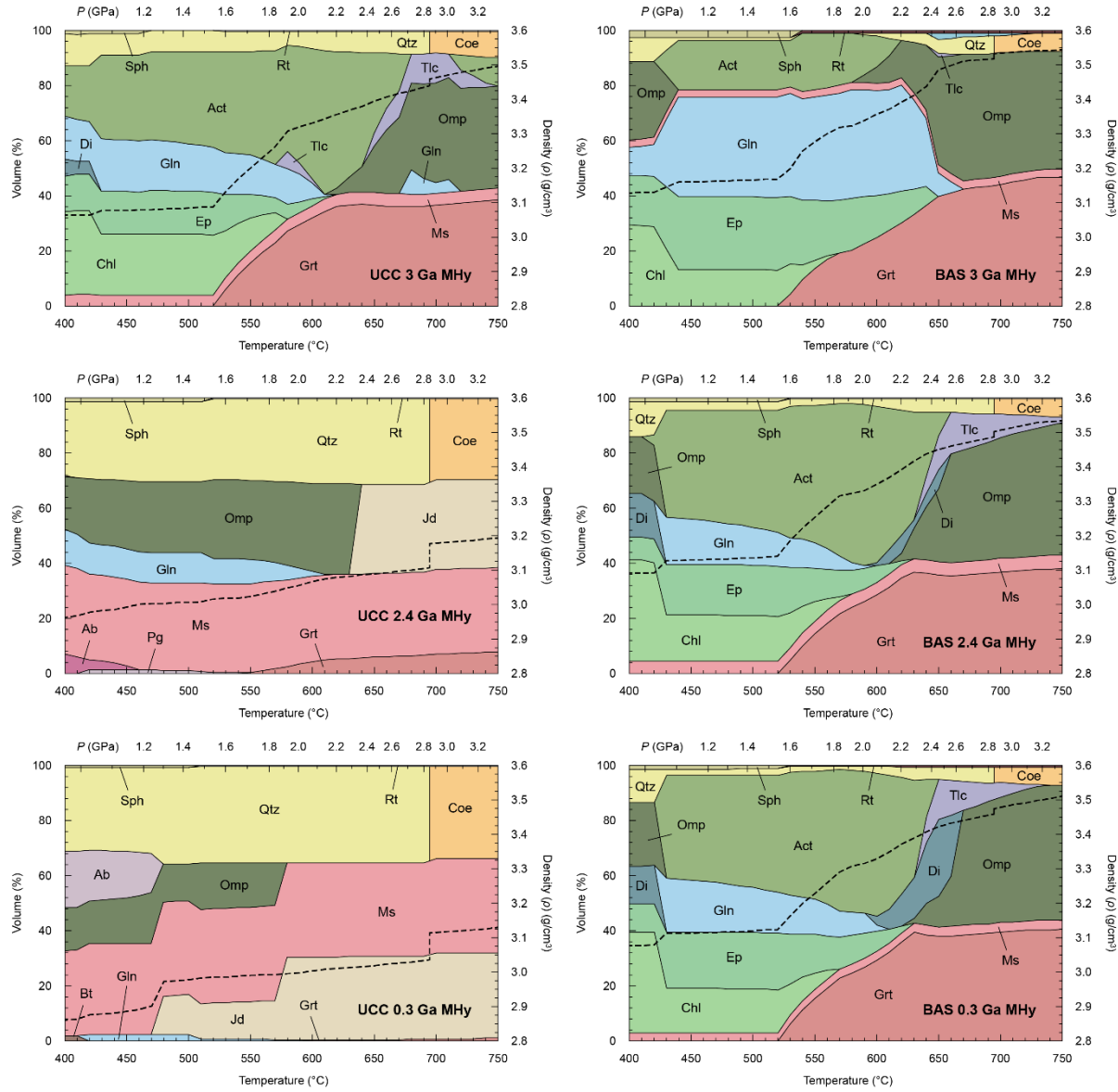
12   \*Corresponding author: richard.palin@earth.ox.ac.uk

## 13 MONTE CARLO SENSITIVITY ANALYSIS

14 Checks on the validity of our petrological modeling results were performed by applying a Monte  
15 Carlo sensitivity analysis to the error in proportions of ultramafic (komatiite), mafic  
16 (greenstone), and felsic (TTG gneiss) components reported by Chen et al. (2020) for  
17 Mesoarchean UCC. These ranges were: 0–36 vol. % (komatiite), 64–75 vol. % (greenstone), and  
18 0–25 vol. % (TTG). We applied the Monte Carlo randomization procedure outlined by Palin et  
19 al. (2016) to generate 500 new estimations of the bulk Archean UCC composition. These spread  
20 mostly between the basalt and basaltic andesite fields on a conventional total alkali–silica (TAS)  
21 diagram (Fig. S4), with some positioned in the picrumbasalt, tephrite, and andesite fields. This  
22 analysis was applied to both anhydrous and minimally hydrated scenarios, as described in the  
23 Methods section of the main manuscript. This procedure was not performed for felsic  
24 Proterozoic or Phanerozoic UCC, given the lower uncertainty of its composition and its strong  
25 negative buoyancy during subduction, as shown in Fig. 3. For the Archean UCC, eight discrete  
26 pressure–temperature ( $P$ – $T$ ) points were considered along the modelled path: 400 °C and 0.95  
27 GPa, 450 °C and 1.16 GPa, 500 °C and 1.42 GPa, 550 °C and 1.72 GPa, 600 °C and 2.07 GPa,  
28 650 °C and 2.46 GPa, 700 °C and 2.90 GPa, and 750 °C and 3.38 GPa.

29 Box and whisker plots (Fig. S5) for each of these  $P$ – $T$  conditions demonstrate that crustal  
30 composition determined by Chen et al. (2020) using a komatiite–basalt–felsic rock ratio of  
31 20:69:11 (Table S1) is representative of the total range as defined by their calculated errors,  
32 showing densities correlating more or less with the 50<sup>th</sup> percentile of the randomized set in each  
33 case. The calculated ‘point of no return’ for minimally hydrated Archean UCC discussed in the  
34 main manuscript, which occurs at ~2.3 GPa (Fig. 3), is reproduced by this sensitivity analysis  
35 (cf. Fig. S5). At slightly lower pressure, between 0% and 28% of all randomized bulk  
36 compositions exhibit negative buoyancy, although above 2.4 GPa, between 73% and 92% are  
37 denser than surrounding mantle pyrolite. For anhydrous equivalents, very few randomized  
38 examples retain positive buoyancy compared to mantle pyrolite: from 22% to 33% below the  
39 quartz–coesite transition, and less than 19% above the transition. These data suggest that some  
40 highly felsic crust may have the potential to be exhumed from Archean subduction zones without  
41 the help of external forcing, although this is not expected to be the norm.

42 **FIGURES**

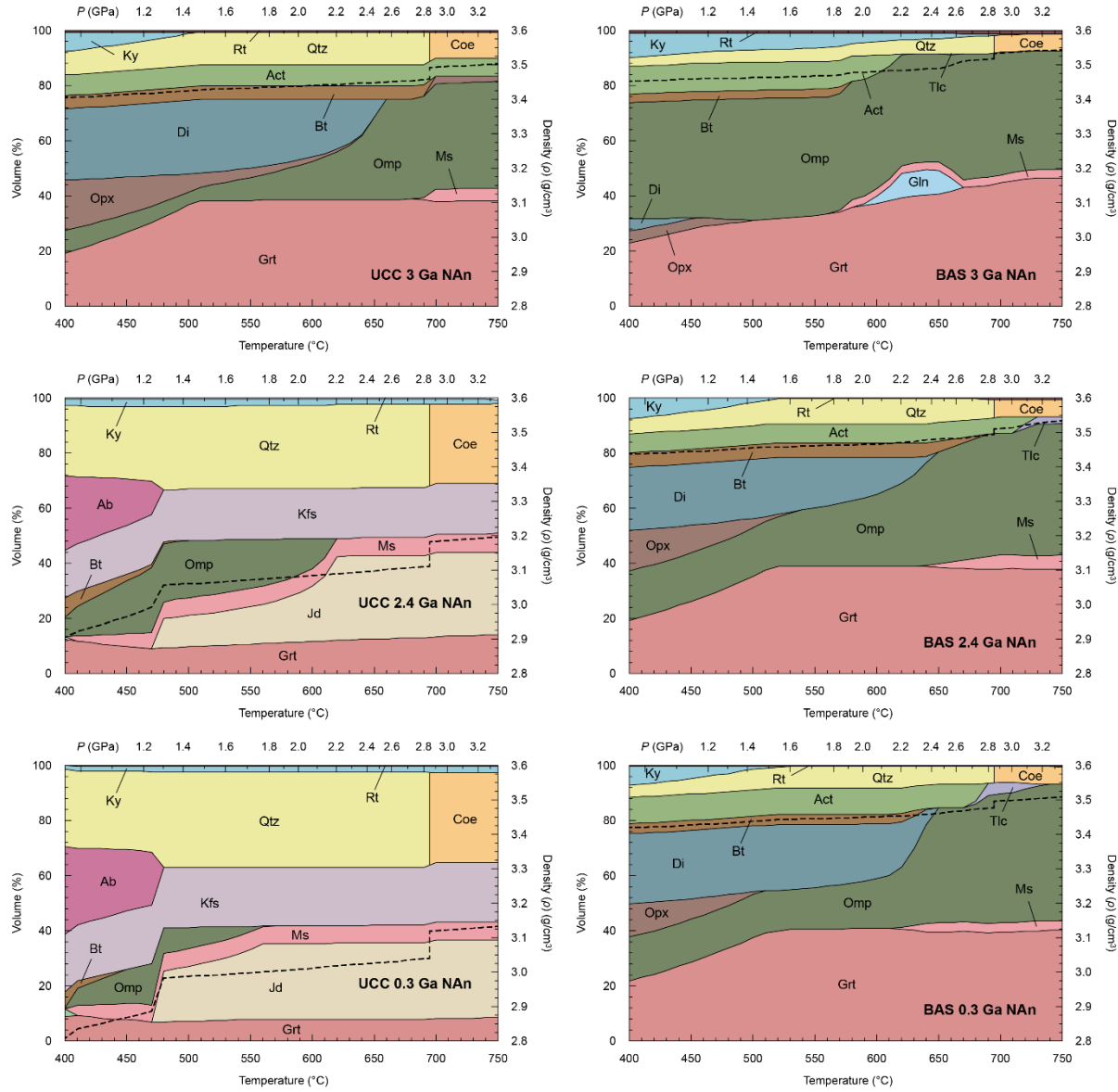


43

44

45 **Figure S1.** Modeboxes for minimally hydrated (MHy) crustal lithologies at 0.3, 2.4, and 3 Ga showing equilibrium volume proportions of solid phases stable along the modeled geotherm. Free aqueous fluid content is not shown, as it does not affect bulk-rock density. UCC = Upper continental crust and BAS = continental basalt. See Table 3 for bulk compositions. Bold dashed line shows bulk-rock density and mineral abbreviations are after Whitney and Evans (2010).

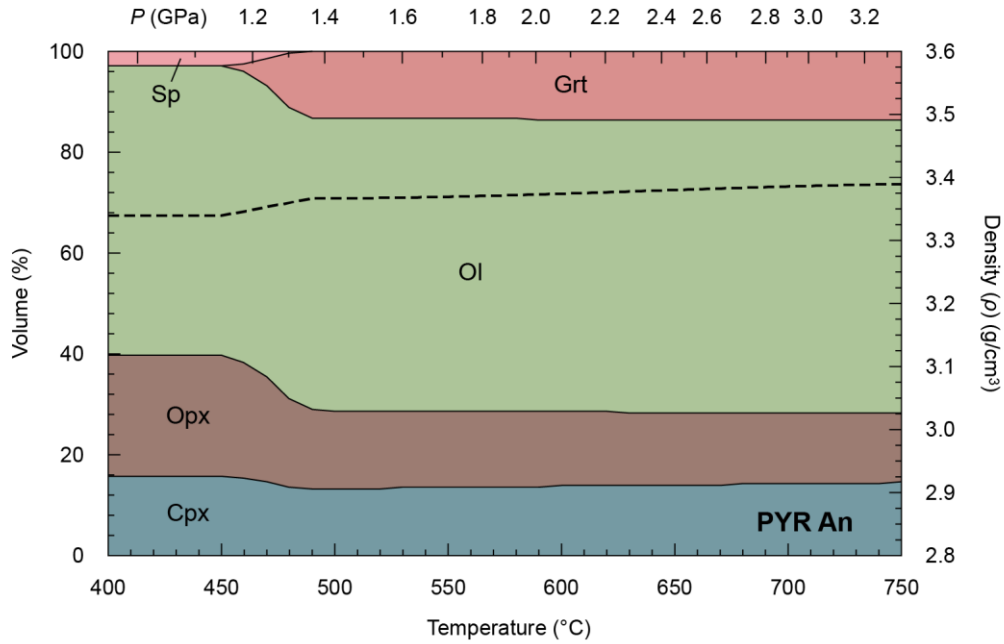
46



51

52

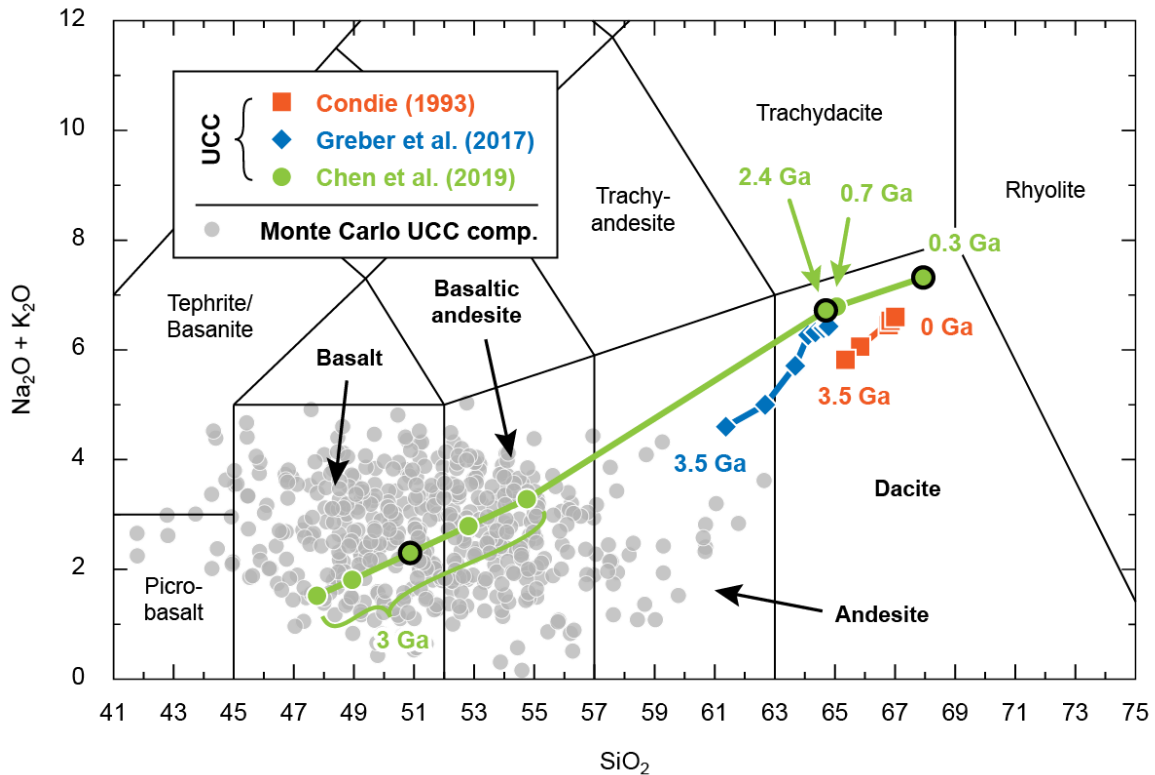
53 **Figure S2.** Modeboxes for nominally anhydrous (NAn) crustal lithologies at 0.3, 2.4, and 3 Ga  
 54 showing equilibrium volume proportions of solid phases stable along the modeled geotherm.  
 55 Free aqueous fluid content is not shown, as it does not affect bulk-rock density. UCC = Upper  
 56 continental crust and BAS = continental basalt. See Table 3 for bulk compositions. Bold dashed  
 57 line shows bulk-rock density and mineral abbreviations are after Whitney and Evans (2010).



58

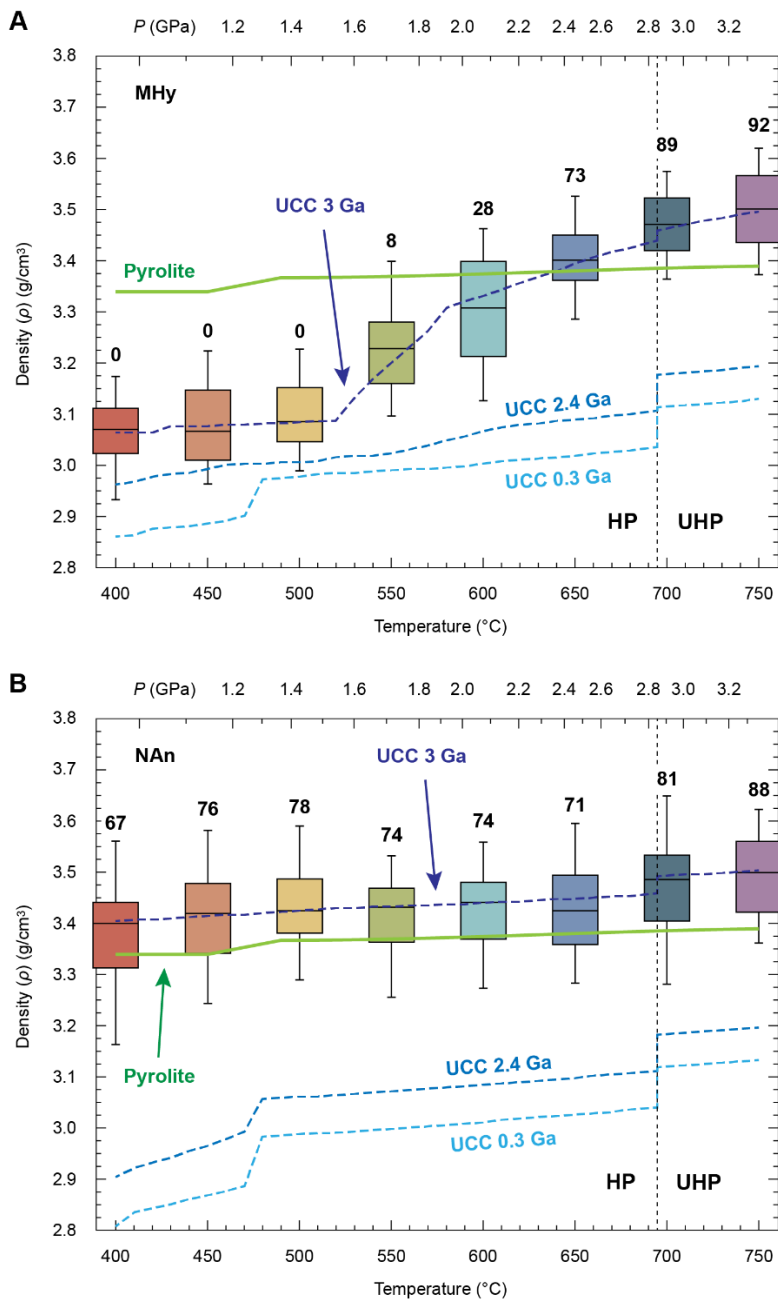
59

60 **Figure S3.** Modebox for anhydrous pyrolite (PYR An) showing equilibrium volume proportions  
 61 of phases stable along the modeled geotherm. Bold dashed line shows bulk-rock density and  
 62 mineral abbreviations are after Whitney and Evans (2010).



63

64 **Figure S4. Total alkali–silica (TAS) diagram showing calculated distribution of**  
 65 **randomized Archean (3 Ga) UCC bulk compositions used for sensitivity analysis.** The  
 66 Monte Carlo procedure (cf. Palin et al., 2016) produced 500 new compositions for Archean UCC  
 67 (grey circles) by considering errors reported by Chen et al. (2020) for all three major lithological  
 68 components: komatiite, greenstone (basalt), and felsic crust (TTG). These data mostly occupy  
 69 the basalt and basaltic andesite fields on the TAS diagram. These 500 data points were used to  
 70 generate the density distributions at each pressure–temperature condition shown in Fig. S5.



71

72 **Figure S5. Results of sensitivity analysis for the density of Archean (3 Ga) UCC during**  
 73 **subduction.** Density distributions are shown as box and whisker plots and consider 500  
 74 randomized bulk compositions determined at eight pressure–temperature ( $P$ – $T$ ) conditions (see  
 75 Supplementary Information text). The upper and lower limits of each box are the 75<sup>th</sup> and 25<sup>th</sup>  
 76 percentiles, respectively, the 50<sup>th</sup> percentile is the line within the box, and the whiskers represent  
 77 the 5<sup>th</sup> and 95<sup>th</sup> percentiles. Numbers above each box show the percentage of data points for that  
 78  $P$ – $T$  condition that have a density greater than surrounding pyrolite. All other annotations are  
 79 taken from Fig. 3 in the main text.

80 **TABLES**

81 **Table S1.** Upper continental crust (UCC) compositions (weight % oxide) reconstructed by Chen et al. (2020), reported on an anhydrous basis  
 82 with all iron as  $\text{Fe}^{2+}$ . The Archean UCC composition considered here is for a komatiite–basalt–felsic rock ratio of 20:69:11. Interpreted juvenile  
 83 continental crust thickness is from Dhuime et al. (2015). The UCC is taken to represent the top third of the entire crustal column.

Age (Ga)	Thickness (km)	$\text{SiO}_2$	$\text{TiO}_2$	$\text{Al}_2\text{O}_3$	$\text{FeO}^{\text{tot}}$	$\text{MnO}$	$\text{MgO}$	$\text{CaO}$	$\text{Na}_2\text{O}$	$\text{K}_2\text{O}$	$\text{P}_2\text{O}_5$
Archean (3)	18	50.87	0.69	12.19	11.47	0.18	11.14	8.14	1.86	0.44	0.07
Paleo-Proterozoic (2.4)	25	64.70	0.69	14.84	5.33	0.08	2.26	3.86	3.48	3.24	0.17
Phanerozoic (0.3)	32	67.94	0.50	14.66	4.04	0.07	1.34	2.70	3.59	3.72	0.14

84

85 **Table S2.** Bulk-rock compositions used for petrological modeling (mol. %). Upper continental crust (UCC) compositions after Chen et al.  
 86 (2020) (cf. Table 1), basalt/greenstone compositions after Condie et al. (2016), and pyrolite composition after Ringwood (1975). MHy =  
 87 minimally hydrated; NAn = nominally anhydrous.

Age (Ga)	Petrological component	$\text{H}_2\text{O}$	$\text{SiO}_2$	$\text{Al}_2\text{O}_3$	$\text{CaO}$	$\text{MgO}$	$\text{FeO}$	$\text{K}_2\text{O}$	$\text{Na}_2\text{O}$	$\text{TiO}_2$	O
Archean (3)	UCC (NAn)	1.00	52.44	7.41	8.99	17.11	9.89	0.29	1.86	0.54	0.49
	UCC (MHy)	13.01	46.07	6.51	7.90	15.03	8.69	0.25	1.64	0.47	0.43
	Basalt/greenstone (NAn)	1.00	51.07	9.76	11.27	14.11	8.27	0.18	2.90	1.04	0.41
	Basalt/greenstone (MHy)	13.76	44.48	8.50	9.82	12.29	7.20	0.16	2.53	0.90	0.36
Paleo-Proterozoic (2.4)	UCC (NAn)	1.00	69.94	9.45	4.47	3.65	4.82	2.23	3.65	0.56	0.24
	UCC (MHy)	12.27	61.97	8.38	3.96	3.23	4.27	1.98	3.23	0.50	0.21
	Basalt/greenstone (NAn)	1.00	51.12	7.41	10.70	17.31	9.33	0.31	1.81	0.54	0.48
	Basalt/greenstone (MHy)	13.75	44.53	6.46	9.32	15.08	8.13	0.27	1.57	0.47	0.42
Phanerozoic (0.3)	UCC (NAn)	1.00	73.73	9.37	3.13	2.17	3.66	2.58	3.78	0.40	0.18
	UCC (MHy)	9.91	67.09	8.53	2.85	1.97	3.33	2.35	3.44	0.37	0.16
	Basalt (NAn)	1.00	50.86	7.72	11.11	16.75	9.47	0.22	1.94	0.47	0.49
	Basalt (MHy)	13.75	44.30	6.72	9.68	14.59	8.24	0.19	1.69	0.41	0.43

88

89 **Table S3.** Parameters used for isostatic balance calculations.

Symbol	Parameter	Archean	Proterozoic
$\rho_w$	Density of seawater	1030 kg m <sup>-3</sup>	1030 kg m <sup>-3</sup>
$\rho_o$	Density of continental crust	2865 kg m <sup>-3</sup>	2800 kg m <sup>-3</sup>
$\rho_c$	Density of oceanic crust	2900 kg m <sup>-3</sup>	2900 kg m <sup>-3</sup>
$\rho_m$	Density of mantle	3330 kg m <sup>-3</sup>	3330 kg m <sup>-3</sup>
$h_o$	Ocean depth above Proterozoic oceanic crust	—	4 km
$T_o$	Thickness of oceanic crust	7 km	7 km
$T_c$	Thickness of continental crust	18 km	30 km
$\lambda$	Fraction of basalt in Archean continental crust	0.65	—

91 **REFERENCES**

92 Chen, K. *et al.* How mafic was the Archean upper continental crust? Insights from Cu and Ag  
93 in ancient glacial diamictites. *Geochim. Cosmochim. Acta* **278**, 16–29 (2020).

94 Condie, K.C., Aster, R.C., & Van Hunen, J. A great thermal divergence in the mantle  
95 beginning 2.5 Ga: Geochemical constraints from greenstone basalts and komatiites.  
96 *Geosci. Front.* **7**, 543–553 (2016).

97 Dhuime, B., Wuestefeld, A., & Hawkesworth, C.J. Emergence of modern continental crust  
98 about 3 billion years ago. *Nature Geosci.* **8**, 552–556 (2015).

99 Palin, R.M., Weller, O.M., Waters, D.J., & Dyck, B. Quantifying geological uncertainty in  
100 metamorphic phase equilibria modelling; a Monte Carlo assessment and implications  
101 for tectonic interpretations. *Geosci. Front.*, **7**, 591–607 (2016).

102 Ringwood, A.E. Composition and Petrology of the Earth's Mantle. MacGraw-Hill, 618  
103 (1975).

104 Whitney, D.L., & Evans, B.W. Abbreviations for names of rock-forming minerals. *Am.*  
105 *Mineral.* **95**, 185–187 (2010).